Braun, Doris E.; Lampl, Martin; Kahlenberg, Volker; Wurst, Klaus; Schottenberger, Herwig; Hummel, Michael; Griesser, Ulrich J.

2-Mercaptoimidazolium halides : structural diversity, stability and spontaneous racemisation

Published in:
CrystEngComm

DOI:
10.1039/d0ce00774a

Published: 28/09/2020

Document Version
Peer-reviewed accepted author manuscript, also known as Final accepted manuscript or Post-print

Please cite the original version:
Braun, D. E., Lampl, M., Kahlenberg, V., Wurst, K., Schottenberger, H., Hummel, M., & Griesser, U. J. (2020). 2-Mercaptoimidazolium halides : structural diversity, stability and spontaneous racemisation. *CrystEngComm*, *22*(36), 6034-6046. https://doi.org/10.1039/d0ce00774a

ARTICLE

2-Mercaptoimidazolium halides: structural diversity, stability and spontaneous racemisation

Received 00th January 20xx,
Accepted 00th January 20xx

DOI: 10.1039/x0xx00000x

Doris E. Braun,*[a] Martin Lampl,[b] Volker Kahlenberg,[c] Klaus Wurst,[b] Herwig Schottenberger,[b] Michael Hummel[d] and Ulrich J. Griesser[a]

Experimental and theoretical characterisations and studies of the stability of heterobicyclic thiazinium salts (bicyclic 2-mercaptoimidazolium chlorides and bromides) were performed to rationalise and understand the influence of the counterion ($Cl^- \leftrightarrow Br^-$) and the replacement of CH by N on crystal packing, the influence of the anion on the moisture and temperature dependent stability, and the racemisation behaviour of the imidazo-thiazinium chloride. Six compounds were synthesised and for five of the compounds the structures were solved from single-crystal X-ray diffraction data. The structural features of the sixth compound could be derived from powder X-ray diffraction data comparisons. An exchange of the Cl^- anion by Br^- does not influence the crystal packing of the racemic thiazinium salt but increases its moisture dependent stability. In contrast, replacing the imidazole moiety of the cation by a triazole or tetrazole moiety results in distinct packing arrangements of the investigated bromide salts, although, substitution calculations suggest that isostructural packing arrangements might exist. The binary melting point phase diagram was constructed to confirm the nature of the racemic species of the thiazinium chloride, and differential scanning calorimetry and lattice energy minimisations were used to estimate the enthalpy difference between the racemic and enantiopure crystals, rationalising the high tendency of racemisation of the enantiopure compound.

1. Introduction

Numerous fine-chemicals are chiral and exist as racemic solids. A racemic mixture of a chiral molecule can exist in the solid-state as a racemic crystal (both enantiomers in the unit cell in equal stoichiometry), a conglomerate (mechanical mixture of equimolar quantity of the two homochiral crystals), or, more rarely, a racemic solid solution (both enantiomers in the unit cell but with no fixed stoichiometry; mixed crystal, pseudoracemate). The racemic crystal is the most common phase among racemates (approx. 90%), followed by conglomerates (approx. 10%) and solid solutions (<1%).[1] Each of the three types of racemic solids can be polymorphic[2] or form solvates.[3] However, it is often not obvious whether two specific solid-state forms of a racemic mixture are polymorphs of the same type (e.g. two polymorphs of a racemic compound) or different types (e.g. racemic compound and conglomerate) and therefore such a distinction is often disregarded. According to Dunitz[4] a conglomerate and a racemate should be only regarded as polymorphs if the interconversion of the two enantiomers in the melt or solution is fast, but since the racemisation time frame is not clearly defined,[5] "pragmatic solutions" in the terminology of such solid-state forms seem to be justified.

The nature of the racemic solid defines to a large extend the crystallisation process employed.[6-9] Control of chiral crystallisation has long been of great industrial interest,[10-13] particularly after the 1992 FDA guideline stipulating that racemates of new stereoisomeric drugs should only be developed to a final product if the enantiomers show only little differences in their pharmacological, pharmacokinetic and toxicological profile.[14]

Ever since the discovery of imidazoles,[15] the scientific world is still intrigued by this simple aromatic molecule. Azolium heterocycles are not only present in natural products, but also in countless substances of technical and medicinal importance.[16-22] The 2-thionated derivatives show valuable biological, e.g. anti-thyroid, properties.[23-25] The incorporation of a thiazine ring by *S*-alkylative cyclisation with halohydrins results in imidazo-thiazine or imidazo-thiazinium compounds, which have been proven to show physiological activity.[26] Despite of the fact that imidazo-, triazolo- or tetrazolo-thiazines and thiazinium salts are currently extensively researched,[26-30] only a few crystal structures have been reported in the literature.[31-35] Besides their biological properties, thiazine compounds are also key intermediates for thiiranes due to their ability to undergo recyclisation reactions.[36, 37]

[a] *Institute of Pharmacy, University of Innsbruck, Innrain 52c, 6020 Innsbruck, Austria; E-Mail: doris.braun@uibk.ac.at.*
[b] *Institute of General, Inorganic and Theoretical Chemistry, Innrain 80-82, University of Innsbruck, 6020 Innsbruck, Austria.*
[c] *Institute of Mineralogy and Petrography, Innrain 52, University of Innsbruck, 6020 Innsbruck, Austria.*
[d] *Aalto University, School of Chemical Engineering, Department of Bioproducts and Biosystems, P.O. Box 16300, 00076 Aalto, Finland.*

† Electronic Supplementary Information (ESI) available: NMR and IR spectra, single crystal X-ray diffraction, conformational analysis, Crystal16 solubility determinations, CrystalExplorer pairwise interaction energy calculations, and lattice energy substitution calculations. CCDC deposition numbers: 2006014-2006018. See DOI: 10.1039/x0xx00000x

Understanding basic physico-chemical properties of any chemical substance is crucial for its design, handling and application. Therefore, our research focused on the preparation, stability as well as the physico-chemical and crystallographic characterisation of thiazinium salts (Fig. 1).

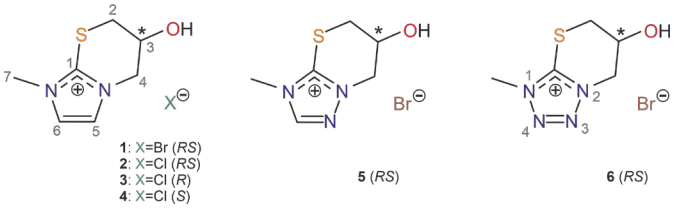

Fig. 1. Molecular structures of the thiazinium salts investigated in this study, incl. the atom numbering scheme for carbon and nitrogen atoms. The '*' marks the chiral carbon atom.

Solid-state characterisations of fine-chemicals can be performed with a wide range of complementary analytical techniques.[38, 39] There exists no single superior method for all systems or investigations, and the methods of choice depend on the key properties of interest. Usually, the preferred approach is to apply a combination of techniques, as each provides unique information about solid forms.[40] In this study we aimed to address (i) the structural diversity among the investigated thiazinium salts, (ii) the stability of the enantiopure imidazo-thiazinium chloride in comparison with the racemic crystal, (iii) the influence of the counterion (Cl^- vs. Br^-) on temperature and moisture dependent stability of isostrucutral salts, and (iv) the influence of chemical variation of the aromatic core (***1***, ***5*** and ***6***, Fig. 1) on crystal packing. Therefore, various experimental techniques and computational modelling were employed to reveal the structural and stability features of the chosen thiazinium salts, including single-crystal (SCXRD) and powder X-ray diffraction (PXRD), moisture sorption experiments, differential scanning calorimetry (DSC), hot-stage microscopy (HSM) and solubility measurements. The experiments were complemented with the generation of the binary melting point phase diagram of ***2*** and its two enantiomers ***3*** and ***4***, pairwise intermolecular energy and lattice energy/substitution calculations.

2. Results and Discussion

2.1. Synthesis of thiazinium compounds

As mentioned introductorily, the racemic thiazinium bromide (*RS*-**Br**, ***1***), the isostructural chloride (*RS*-**Cl**, ***2***), and triazole (***5***) and tetrazole (***6***) based bromide salts have been synthesised using (*rac*)-epibromohydrin or (*rac*)-epichlorohydrin as *S*-alkylating agents forming a quaternised heterocycle with 2-mercapto-1-methylimidazole (methimazole), 3-mercapto-4-methyl-4*H*-1,2,4-triazole or 5-mercapto-1-methyltetrazole, respectively (Scheme 1).

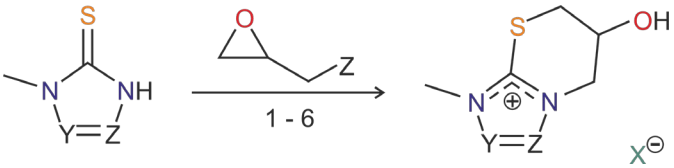

Scheme 1. Synthetic approach to thiazinium systems based on mercaptoimidazole, -triazole and -tetrazole. (***1***) $CHCl_3$, X = Br, Y,Z = CH; (***2***) MeCN, X = Cl, Y,Z = CH; (***3***, ***4***) MeCN (anhydrous) X = Cl, Y,Z = CH; (***5***) MeCN, X = Br, Y = CH, Z = N; (***6***) MeCN, X = Br, Y,Z = N.

The enantiopure product in *R*-configuration of the chloride (**R**-*Cl*, ***3***) was obtained by using (*S*)-epichlorohydrin, the *S*-enantiomer (**S**-*Cl*, ***4***) by using (*R*)-epichlorohydrin. The reaction took place in anhydrous solvents applying standard Schlenk-techniques.

All substances, with the exception of ***4*** (*S*-**Cl**) crystallised readily and their structures could be determined from single-crystal X-ray diffraction data (see next section). Compound ***4*** was obtained in crystalline form, but the size of the crystals did not allow a structure determination using laboratory SCXRD equipment. As the structure of the *R*-enantiomer was solved and the PXRD patterns of the *S*- and *R*-enantiomers were identical, no further efforts were undertaken to solve the structure. The PXRD patterns simulated from the single crystal structures proved to agree with the PXRD measurements of the respective bulk samples when considering thermal effects on the peak positions.

2.2. Structural features of thiazinium compounds

(*RS*)-6-Hydroxy-1-methyl-1,5,6,7-tetrahydroimidazo[2,1-b][1,3]thiazinium bromide (RS-*Br*, *1*) and **(*RS*)-6-hydroxy-1-methyl-1,5,6,7-tetrahydroimidazo[2,1-b][1,3] thiazinium chloride (RS-*Cl*, 2).** The two racemic imidazo-thiazinium salts crystallise in the monoclinic *C*2/*c* space group (Table S1, ESI) and each one cation and one anion is present in the asymmetric unit. A comparison of the lattice parameters and packing diagrams of the two compounds reveals that the Br^- and Cl^- salts are isostructural (Fig. 2),[41] with the cations exhibiting a $rmsd_{15}$[42] value of 0.14 Å. The cations are located on planes parallel to (1 0 1), with both hands being present in one plane (related by inversion symmetry). The anions (Br^- or Cl^-) are located in the same planes and form strong ionic hydrogen bonding interactions to the hydroxyl group of the cations of adjacent planes, and thus, connect the planes into a 3D packing motif. In addition to the O–H···X^- (X = Br or Cl) interaction also C–H···X^- close contacts stabilise the racemic salt packings. Each of the X^- ion is coordinated by seven thiazinium anions within a 5 Å radius (optimised PBE-TS structure used to allow comparisons with the other compounds).

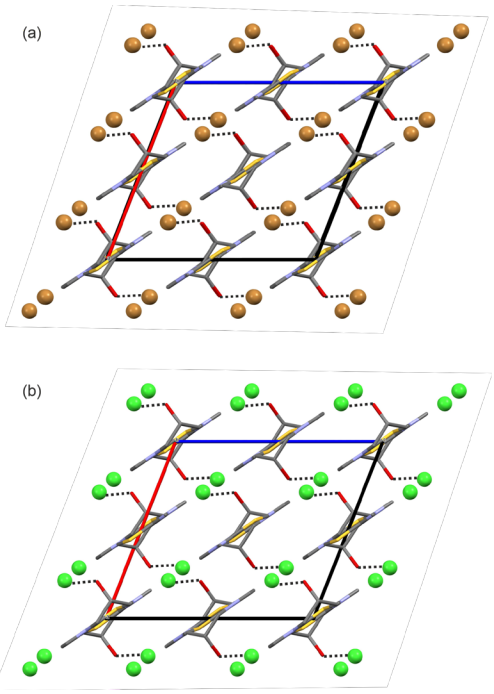

Fig. 2. Packing diagrams of (a) *RS*-**Br** (***1***) and (b) *RS*-**Cl** (***2***) viewed along the *b* crystallographic axes. Hydrogen atoms have been omitted for clarity and Cl⁻···O–H interactions are indicated with dotted lines.

The pairwise interaction energies were calculated using CrystalExplorer and are exemplarily shown for *RS*-**Cl** (***2***) in Fig. 3a as energy frameworks diagrams.[43]

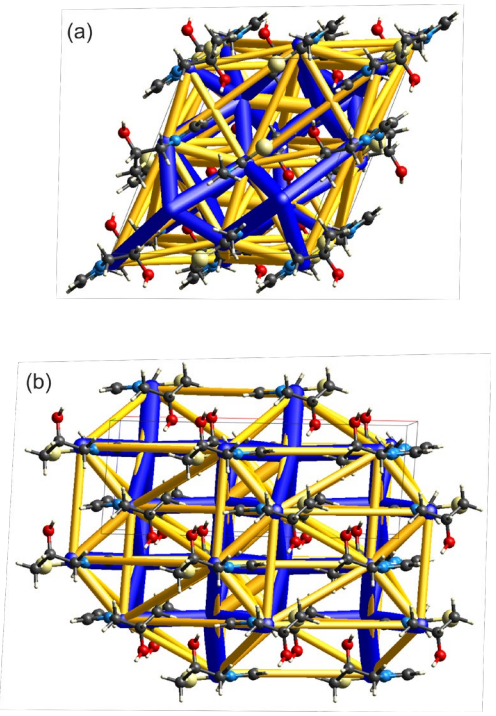

Fig. 3. Energy framework diagrams (total energy) for (a) ***2*** and (b) ***3*** viewed along the *b* crystallographic axes. The energy scale factor is 15. Stabilising (negative pairwise interactions) and destabilising (positive pairwise interactions) contacts are shown in blue and yellow, respectively. For more details, see Table S2, ESI.

The strong ionic interactions (O–H···Cl⁻ and C–H···Cl⁻) were estimated to account for –401.5 kJ mol⁻¹ to –290.0 kJ mol⁻¹ in pairwise interaction energy. As expected, the strongest interaction arises from the O–H···Cl⁻ contact (for more details see section 4 of the ESI).

(*R*)-6-Hydroxy-1-methyl-1,5,6,7-tetrahydroimidazo[2,1-b][1,3]thiazinium chloride (*R*-Cl, *3*). Upon exposing the enantiopure crystals to moisture (RT), *i.e.* removal from its mother liquid, deliquescence and racemisation (*R* → *RS*) occurred within seconds to minutes. The same is also true for the *S*-enantiomer. The latter information was crucial for handling the samples.

The enantiopure crystals adopt the monoclinic *C*2 space group symmetry, with Z'=1. In contrast to the racemic crystals, the cations are arranged in a slightly tilted orientation in planes parallel to (0 0 4) in the homochiral crystal (Fig. 4a). The Cl⁻ anions are located on the same planes and strongly interact with the hydroxyl function of the cation of an adjacent plane. Similar to the racemic crystal, the Cl⁻ ion is coordinated by seven thiazinium cations within a 5 Å radius and O/C–H···Cl⁻ close contacts significantly contribute to the stability of the homochiral crystal structure (Fig. 3b). The latter interactions, O–H···Cl⁻ and C–H···Cl⁻, were calculated as –383.2 kJ mol⁻¹ to –267.0 kJ mol⁻¹ in pairwise interaction energy.

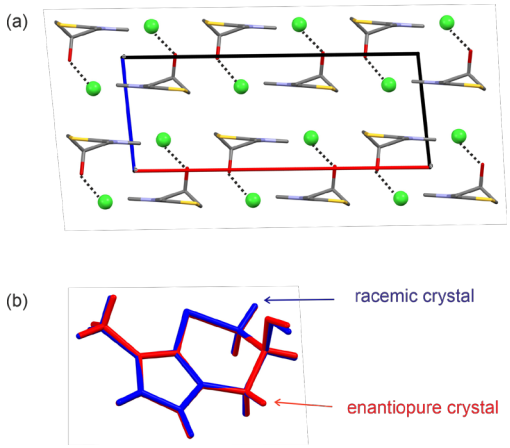

Fig. 4. (a) Packing diagram *R*-**Cl** (**3**) viewed along the *b* crystallographic axis. Hydrogen atoms have been omitted for clarity and Cl⁻···O–H interactions are indicated with dotted lines. (b) Overlay of the conformation present in the racemic (***1***,***2*** – in blue) and enantiopure (***3*** – in red) crystals.

A comparison of the racemic and homochiral imidazo-thiazinium chlorides total energy frameworks (Fig. 3) suggests that the homochiral crystal shows a lower stability due to "weaker" stabilising intermolecular interactions and also due to a lower packing efficiency as is evident from the higher density of the racemic crystals. Thus, 6-hydroxy-1-methyl-1,5,6,7-tetrahydroimidazo[2,1-b][1,3]thiazinium chloride conforms to Wallach's rule as the racemic compound is denser than the enantiomeric crystal.[44] The relative stability difference between the homochiral and racemic crystals will be addressed in section 3.4.

The potential energy scans for the 6-hydroxy-1-methyl-1,5,6,7-tetrahydroimidazo[2,1-b][1,3]thiazinium cation, starting from two low energy ring conformations (Fig. 5a), and varying the H–O–C3–C4 dihedral angle (Fig. 1) reveals that the cation exhibits several low energy conformations and that the hydroxyl group can rotate

considerably with low cost in intramolecular energy (E_{intra}). Surprisingly, the conformations found in ***1*** – ***3*** are nearly superimposable (Fig5b), with the H–O–C3–C4 dihedral angle varying only by 5.4°. The conformation found in the three structures is not related to the global minimum conformation, but related to a local minimum which is ≤ 5 kJ mol^{-1} higher in energy than the global minimum, calculated at different levels of theory (marked with ***1*** – ***3*** in Fig. 5b).

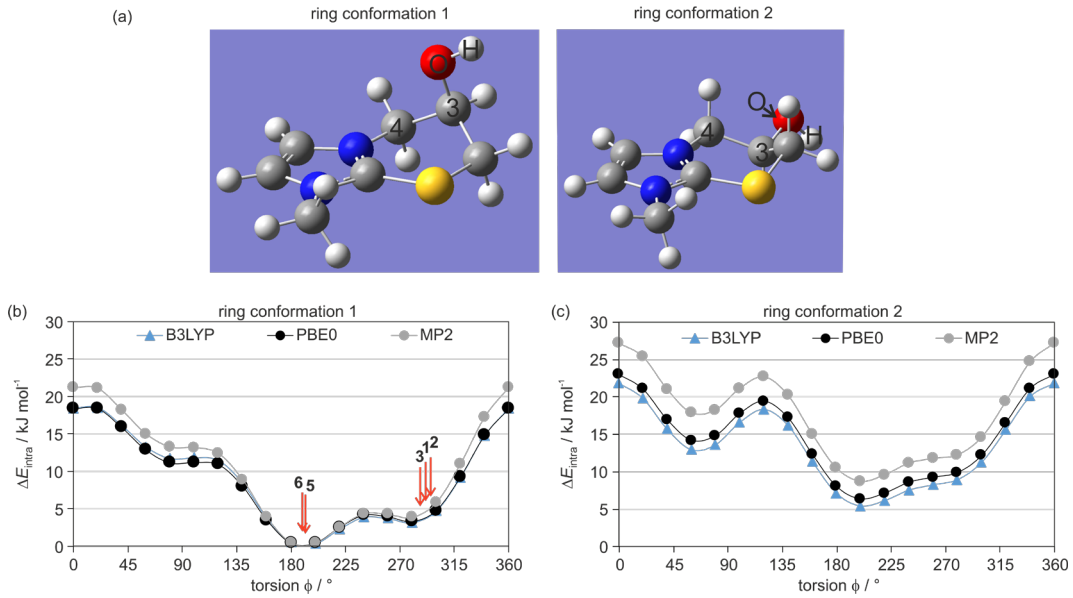

Fig. 5. (a) Low energy aliphatic ring conformations of thiazinium cations, which were used as starting points for the potential energy scans depicted in (b and c). The intramolecular energy differences (ΔE_{intra}) were calculated at the B3LYP/6-31G(d,p), PBE0/6-31G(d,p) and MP2/6-31G(d,p) levels of theory. Additional PES scans are given in section 3 of the ESI.

(*RS*)-6-Hydroxy-3-methyl-3,5,6,7-tetrahydro-[1,2,4]triazolo[5,1-b][1,3]thiazinium bromide (*5*). The compound crystallises in the orthorhombic space group *Pna*2$_1$, with Z'=1. The anion and cations are located in corrugated layers and are connected via an O–H···Cl$^-$ interaction (Fig. 6a). The layers are related by 2$_1$ screw axes and glide plane symmetry to adjacent layers, resulting in homochiral double layer sheets.

Similar to the ***1*** – ***3*** structures, the Br$^-$ forms strong O–H···Br$^-$ and C–H···Br$^-$ interactions to the cation, with the difference that only six cations are located within a five Å range of the Br$^-$, in contrast to seven for the already discussed structures (PBE-TS structures used). Interestingly, there is hardly any difference in the strengths of the O–H···Br$^-$ and strongest C–H···Br$^-$ interactions, which were calculated as –387.7 kJ mol^{-1} and –383.5 kJ mol^{-1}, respectively. For details see section 4 of the ESI. The energy framework diagram (Fig. 6b) indicates that strong interactions are formed within and in between the layers.

The potential energy scans for compound ***5***, given in section 3 of the ESI, generally follow the same trend as the scans for the ***1*** – ***3*** cation (Fig. 5b and c). The H–O–C3–C4 dihedral angle of compound ***5*** can be related to the global minimum. Thus, compared to the ***1*** – ***3*** salt structures not only the packing, but also the conformation of the cation is different for ***5***.

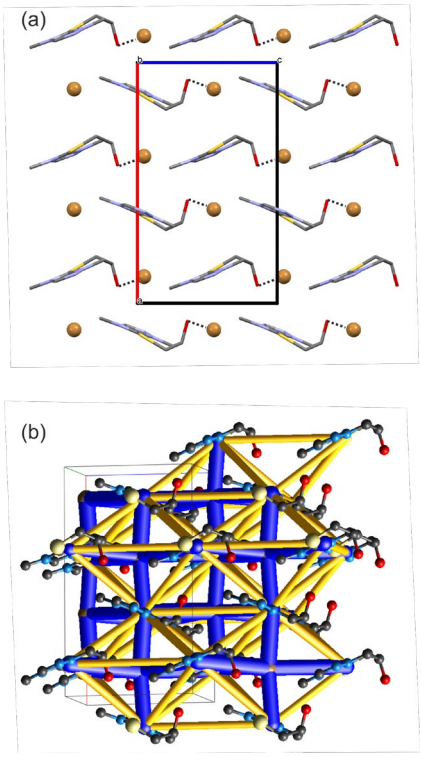

Fig. 6. (a) Packing diagram of ***5*** viewed along the *b* crystallographic axis. O–H···Br$^-$ interactions are denoted with dotted lines. (b) Energy frameworks (total energy): Stabilising (negative pairwise interactions) and destabilising (positive pairwise interactions) contacts are shown in blue and yellow, respectively. The energy scale factor is 15. Hydrogen atoms have been omitted for clarity in (a) and (b). For more details, see Table S2, ESI.

(*RS*)-6-Hydroxy-3-methyl-3,5,6,7-tetrahydrotetrazolo[5,1-b][1,3]thiazinium bromide (*6*). The crystal structure of the third chemically distinct compound adopts the monoclinic $P2_1/c$ symmetry with each one cation and one Br^- in the asymmetric unit. Compounds ***5*** and ***6*** adopt more or less identical orientations of the H–O–C3–C4 dihedral angle, but differ slightly in the deflection of the hydroxylated carbon atom from the plane formed by the five membered ring, with compound ***6*** showing the highest (0.80 Å) and compound ***5*** the lowest value (0.44 Å) of all investigated compounds.

The cations and anions are arranged in layers, comprising the O–H···Br^- interaction (Fig. 7a). Within a layer the configuration is maintained, and each of the two adjacent layers shows the opposite configuration due to inversion or glide plane symmetry relation of adjacent layers. Seven strong close contacts, O–H···Br^- and C–H···Br, are formed within a five Å radius of the Br^- anion (optimised PBE-TS structures). The calculated pairwise interaction energies between the anions and cations range from –394.3 kJ mol^{-1} to –218.8 kJ mol^{-1}, with the O–H···Br^- interaction being the strongest. For more details, see section 4 of the ESI.

A packing comparison of the structures of compounds ***5*** and ***6*** revealed one dimensional packing similarity, *i.e.* identical chains of cations and anions propagating parallel to the *c* axes in the two structures. The same chains are also forming the layers already described for ***5*** and ***6***, although, the layers are not identical. A key difference between ***5*** and ***6*** is the strength of the interactions that interlink the adjacent layers. In ***5*** interlinks are facilitated through the close proximity of the Br^- to each of the two adjacent layers, whereas in ***6*** the inversion relation of adjacent layers does not allow the formation of very strong O–H···Br^- and C–H···Br^- interactions, as clearly visible from the energy framework plot (Fig. 7b).

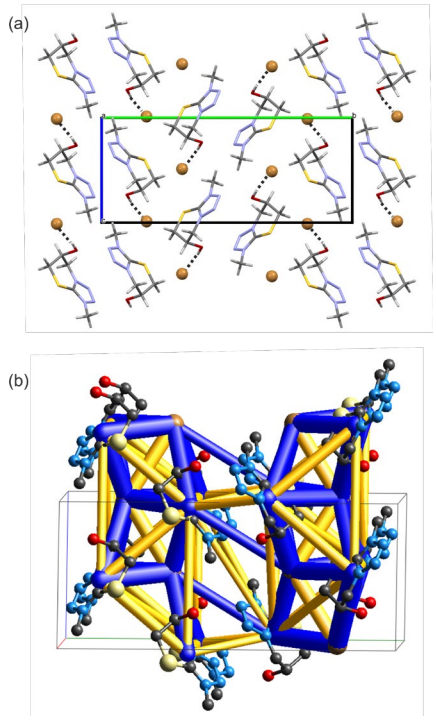

Fig. 7. (a) Packing diagram of ***6*** viewed along the *a* crystallographic axis. O–H···Br^- interactions are denoted with dotted lines. (b) Energy frameworks (total energy): Stabilising (negative pairwise interactions) and destabilising (positive pairwise interactions) contacts are shown in blue and yellow, respectively. The energy scale factor is 15. Hydrogen atoms have been omitted for clarity in (a) and (b). For more details, see Table S2, ESI.

2.3. Influence of the anion on the stability of the salts

The following section investigates the influence of the counterion (Br^- or Cl^-) on the temperature and moisture dependent stability of the compounds, i.e. ***1*** and ***2*** are compared.

Hot-stage microscopy was employed to investigate the behaviour of the two compounds upon increasing temperature. No thermal event was observable except for the melting of the compounds. The Br^- salt shows a slightly lower melting point than the Cl^- salt (Br^-: 172.5 – 174 °C; Cl^-: 178.5 – 179.5 °C). To conclude, the counterion only slightly affects the thermal properties of the salts.

To investigate the influence of the Br^- or Cl^- ions on the moisture dependent stability of the compounds a moisture sorption study was undertaken, starting from ~0% RH at 25 °C (Fig. 8). The two compounds show almost no water uptake up to 50% RH. Above 50% RH *RS*-***Cl*** (***2***) shows deliquescence. In contrast, the bromide salt (***1***) is more resistant with respect to moisture, deliquescence was found to occur only at RH values > 70%. Thus, the exchange of the counterion increases the moisture dependent stability of the Br^- compound relative to its isostructural Cl^- salt. The information derived from the sorption measurements is crucial for being able to handle the two substances at room conditions (20 – 60 % RH), especially for *RS*-***Cl*** (***2***). The substance liquefies and the amount of water uptake depends on the exposure time. No recrystallisation was observed during the desorption cycle of either of the two compounds.

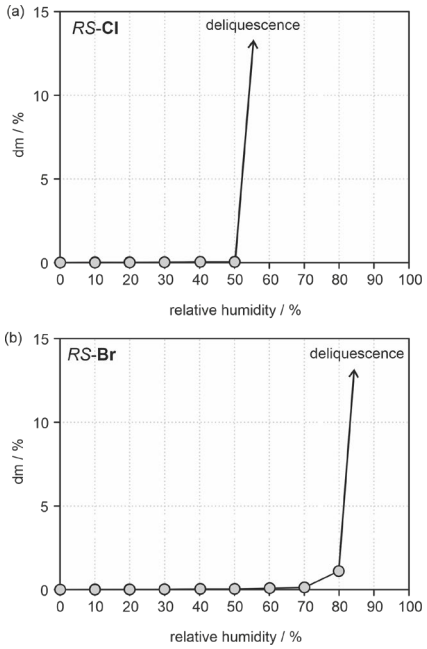

Fig. 8. Gravimetric moisture sorption curves of (a) *RS*-**Cl** (***2***) and (b) *RS*-**Br** (***1***) starting from ~0% RH.

2.4. Thermodynamic comparison of racemic and homochiral imidazo-thiazinium salts.

The thermodynamic relation of the (*R*/*S*)-6-hydroxy-1-methyl-1,5,6,7-tetrahydroimidazo[2,1-b][1,3]thiazinium chloride (***3***, *R*-**Cl** and

4, *S*-**Cl**) to its racemic crystal (***2***, *RS*-**Cl**) was unravelled using experimental and computational approaches.

Racemisation of the *R*-Cl (*3*) and *S*-Cl (*4*) enantiomers. Racemisation of the two enantiomers and the relative stability between the racemic compound and the homochiral crystals were investigated using HSM and PXRD. Allowing the enantiopure crystals to interact with moisture (water) resulted first in deliquescence and then in recrystallisation of the racemic compound, provided the RH is below 40% (for the recrystallisation process). Thus, in solution the following two reactions take place: R(solvated) → RS(solvated) and S(solvated) → RS(solvated). To prevent contact with moisture, which triggers the racemisation reaction, it was necessary to either measure the PXRD patterns of the enantiopure samples between two mylar foils or to cover the solid with anhydrous solvents. The fourth PXRD pattern in Fig. 9 exemplarily shows that the S-enantiomer transformed in the presence of moisture to the racemic crystal within minutes. Thus, at ambient conditions there is a strong thermodynamic driving force for *R*-**Cl** or *S*-**Cl** to racemise to *RS*-**Cl**.

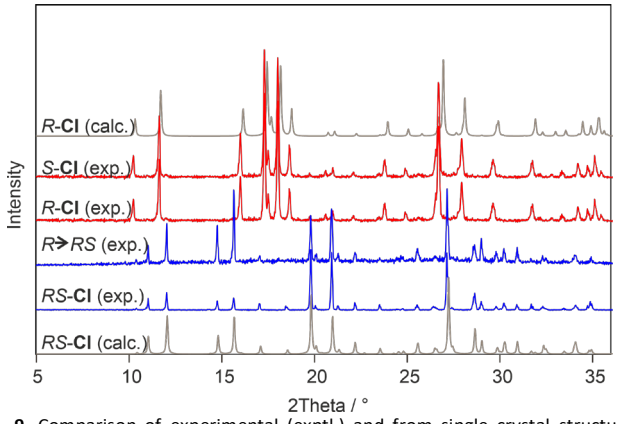

Fig. 9. Comparison of experimental (exptl.) and from single crystal structures simulated (calc.) PXRD patterns.

Relative stability of the racemic compound (*2*). Calorimetric and solubility measurements, as well as lattice energy calculations were employed to determine the stability (enthalpy) of the racemic compound with respect to its enantiopure crystals, i.e. quantify the enthalpy of formation of the racemic compound from its enantiomers, R(crystal) + S(crystal) → RS(crystal).[45]

Differential scanning calorimetry was employed to investigate the thermal behaviour (Fig. 10a) of the imidazo-thiazinium salts and to generate the thermochemical data (Table 1), which were used to calculate the binary phase diagram shown in Fig. 10b. The preparations of the samples and the DSC experiments were performed at driest conditions possible (exclusion of moisture). The DSC curves of the racemic compounds (*RS*-**Br** and *RS*-**Cl**) and single enantiomers (*R*-**Cl** and *S*-**Cl**) exhibit only one distinct endothermic event corresponding the melting process of each compound. In agreement with the HSM investigations, the *RS*-**Cl** shows a higher melting point (178.9 °C) than the Br^- salt (173.5 °C). The enantiopure crystals of the Cl^- salt melt distinctly lower than the corresponding racemic compound (*R*: 126.2 °C, *S*: 126.1 °C). Furthermore, also the heat of fusion is significantly lower for the homochiral crystals than for the racemic compound (Table 1). The energy difference of approx. 19 kJ mol^{-1} indicates a strong tendency towards the formation of the racemic compound. The eutectic temperature between *RS*-**Cl** and *R*-**Cl** (or *RS*-**Cl** and *S*-**Cl**) was measured to be approx. 123 °C by using HSM (samples embedded in silicon oil).

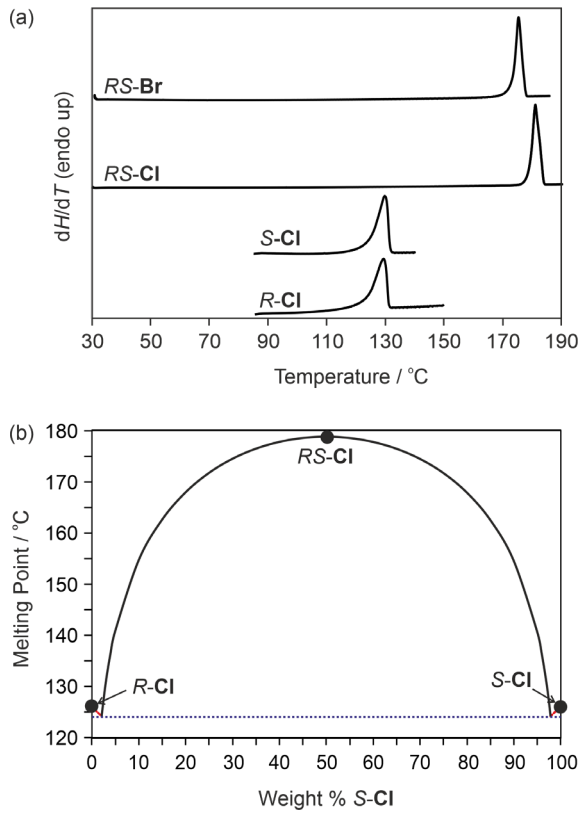

Fig. 10. (a) DSC thermograms of *RS*-**Br**, *RS*-**Cl**, *S*-**Cl** and *R*-**Cl** recorded at a heating rate of 10 °C min^{-1}. (b) Binary melting phase diagram of *R*-**Cl** and *S*-**Cl** showing racemic compound formation. Black circles represent the measured melting point temperatures (with DSC).

Table 1. Values of thermodynamic parameters of *R*-**Cl**, *S*-**Cl** and *RS*-**Cl**.

Compound	*R*-**Cl** (***3***)	*S*-**Cl** (***4***)	*RS*-**Cl** (***2***)	**Δ** (*RS*-*R*), **Δ** (*RS*-*S*)[c]
Thermal Measurements (126 – 174 °C)				
T_{fus}, °C	126.2 ± 1.1	126.1 ± 0.6	178.9 ± 0.1	52.7 ± 1.1, 52.8 ± 0.6
$\Delta_{fus}H$, kJ mol^{-1}	15.1 ± 0.5	15.1 ± 0.5	33.9 ± 0.1	18.8 ± 0.5
$\Delta_{fus}S$, J mol^{-1} K^{-1}	37.8 ± 1.3	37.8 ± 1.3	75.0 ± 0.2	37.2 ± 1.5
Crystal16 Solubility Measurements (20 – 75 °C)				
$\Delta_{sol}H$, kJ mol^{-1}	11.3	10.7	19.7	8.4, 8.9
$\Delta_{sol}S$, J mol^{-1} K^{-1}	13.4	11.5	32.0	18.8, 20.5
Periodic electronic structure calculations (– 273.15 °C), E^{CASTEP}, kJ mol^{-1}				
PBE-TS[a]	–282582.0		–282598.5	–16.5
PBE-D2[a]	–282585.5		–282602.0	–16.5
PBE-MBD*,[b]	–289584.7		–289598.8	–14.1

[a]single point calculations using the PBE-TS optimised structures, [b]fixed cell optimisation using the PBE-TS optimised structures. For details see section 2.9. [c]$\Delta H = -\Delta E^{CASTEP}$.

The binary phase diagram (Fig. 10b) was constructed from the temperatures of the two distinct peaks seen in the DSC traces. The lines indicate the solid-liquid equilibria and assuming that the binary system behaves ideally they were calculated using the equations of Schroeder-Van Laar (2) and Prigogine-Defay (3)[1] in the simplified form:

$$\ln x = \frac{\Delta H_{fus,(S)}}{R}\left(\frac{1}{T_{fus,(S)}} - \frac{1}{T_{fus}}\right) \quad (2)$$

$$\ln 4x(1-x) = \frac{2\Delta H_{fus,(RS)}}{R}\left(\frac{1}{T_{fus,(RS)}} - \frac{1}{T_{fus}}\right) \quad (3)$$

where χ is the mole fraction of one enantiomer of the mixture, R the gas constant (8.314 J K^{-1} mol^{-1}), $T_{fus,(S)}$, $T_{fus,(RS)}$, $T_{fus,(R+S)}$ the melting temperature of the enantiomer, racemic compound and the mixture of R and S, respectively, and $\Delta H_{fus,(S)}$, $\Delta H_{fus,(RS)}$ the enthalpy of fusion of the enantiomer and racemic compound (Table 1). The eutectic point corresponds to the point of intersection of the curves obtained by (1) and (2), calculated to be at 124 °C. Thus, hot-stage microscopy and DSC allowed us to confirm the nature of the racemic compound (Fig. 10b).

Relative stability of the racemic compound from calculations. The stability of the racemic crystal with respect to its homochiral crystals can be estimated from lattice energy calculations.[46, 47] Therefore, periodic electronic structure calculations with the addition of different dispersion correction schemes were employed (Table 1). Independent of the dispersion correction, the racemic crystal (***2***) was calculated to be more stable than the enantiopure crystals (***3*** and ***4***). The potential energy difference was calculated to be 14.1 to 16.5 kJ mol^{-1}, which agrees reasonably well with the thermoanalytical data and proves that lattice energy calculations can be used to estimate stability differences between racemic and homochiral crystals.

Solubility measurements and solution thermodynamics. The experimental solubilities of *RS*-**Br**, *RS*-**Cl**, *R*-**Cl** and *S*-**Cl** were measured between 20 and 75 °C in DMSO using a transmission endpoint determination method (Crystal16). The obtained temperature dependent solubility curves show that the solubility increases with temperature (Fig. 11a&c). Despite carefully handling the samples, minor deliquescence of the homochiral compound may have occurred during the weighing operations, which may have caused some inaccuracy. For all measured samples a linear van't Hoff plot of ln X against 1/T is obtained (Fig. 11b&d). Thermodynamic parameters, the enthalpy of solution (ΔH_{sol}) and entropy of solution (ΔS_{sol}), were estimated from the slope and constant of the regression line of the van't Hoff plot, respectively (Table 1).

The enthalpy of solution can be described as the sum of the a) endothermic heat contributions resulting from breaking up the intermolecular interactions of the solute (crystal lattice) as well as the solvent-solvent interactions and b) the excess heat contributions formed when solute and solvent molecules are mixed (heat of mixing, solvation). If the solvation energy of an enantiomer and the racemic mixture is of similar magnitude, the difference in ΔH_{sol} of the crystalline homochiral phases and the racemic compound should be close to the enthalpy of fusion difference of these solids. The difference between ΔH_{fus} of the racemic compound ***2*** (*RS*-**Cl**) and their enantiomers ***3, 4*** ($\Delta\Delta H_{fus,(RS\text{-}S,\text{ or }RS\text{-}R)}$ = 18.8 kJ mol^{-1}) is about 10 kJ mol^{-1} higher than the corresponding $\Delta\Delta H_{sol}$ value (see Table 2). This suggests that the heat gain of the solvation process of the racemate is roughly twice that of the pure enantiomers and compensates for the stronger solute-solute interactions (lattice energy) of the racemic compound compared to the homochiral crystals.

The comparison of the solubilities of the racemic imidazo-thiazinium salts in DMSO (Fig. 11a&b) shows that the Br$^-$ salt has a higher solubility than the Cl$^-$ salt, which confers with the Br$^-$ compound having a lower melting point and a lower heat of fusion (32.2 ± 0.2 kJ mol^{-1}) than the isostructural Cl$^-$ salt. This is in contrast to the moisture dependent stabilities (Fig. 8). Related studies on ionic liquids (ILs), incl. imidazolium-based ILs, revealed that the Cl$^-$ based ILs show a higher water sorption capacity than the Br$^-$ based ones, which was attributed to the increased strength of hydrogen bonding between water and Cl$^-$.[48, 49] The latter might explain why the Cl$^-$ salt (***2***) shows a higher hygroscopic behaviour than the isostructural Br$^-$ salt (***1***).

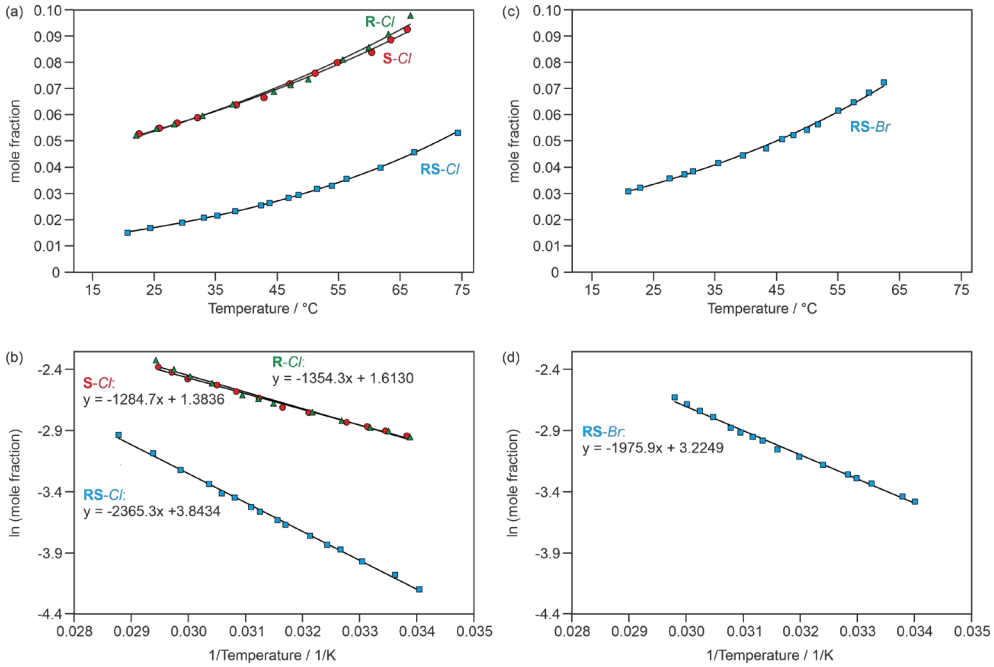

Fig. 11. (a,c) Solubility (mole fraction) of **R**-*Cl*, **S**-*Cl*, **RS**-*Cl* and **RS**-*Br* (imidazo-thiazinium salts) in dimethyl sulfoxide as a function of temperature and (b,d) van't Hoff plot of the molar solubility as a function of temperature.

2.5. Structural diversity amongst thiazinium salts and thermodynamically feasible polymorphs

The structure comparison of the racemic thiazinium bromide salts (***1***, ***4*** and ***5***), which differ only in the number of N atoms, revealed that all three compounds adopt distinct packing arrangements. Only a very limited crystallisation space was considered, *i.e.* crystallisation conditions used for synthesising the compounds and for producing single crystals. Experimental polymorphism screens would have gone beyond the scope of this work. Therefore, we used substitution calculations[50, 51] to investigate whether isostructural racemic bromide salts of the compounds might be observable. Each of the cations of structures ***1***, ***5*** and ***6*** was replaced by the other thiazinium in the same structure and optimised using CASTEP (as described in section 4.9.), resulting in three sets of isostructural packing arrangements: ***1*** – ***5*** in ***1*** – ***6*** in ***1***, ***5*** – ***1*** in ***5*** – ***6*** in ***5***, and ***6*** – ***1*** in ***6*** – ***5*** in ***6*** (see section 6 of the ESI), with $rmsd_{15}$ values[42] (cation only) of 0.08 to 0.68 Å.

A comparison of the lattice energies (Table 2) revealed that some of the computationally generated structures might be observable as polymorphs of the experimental bromide salts. In particular, the experimental structure of ***1*** seems to be a potential alternative packing arrangement for the other two racemic thiazinium salts ***5*** and ***6***. The latter hypothetical polymorphs are thermodynamically feasible, but higher in lattice energy, i.e. less stable (at 0 K).

Table 2. Lattice energies differences of observed and computationally generated (substitution calculations) structures.

Structure	PBE-TS[a]	PBE-D2[b]	PBE-MBD*[,b]
	ΔE_{latt} (kJ mol^{-1})		
	Compound ***1***		
1	0	0	0
1 in ***5***	25.3	24.1	21.3
1 in ***6***	15.6	11.0	10.7
	Compound ***5***		
5	0	0	0
5 in ***1***	2.8	3.4	5.7
5 in ***6***	13.6	12.5	10.7
	Compound ***6***		
6	0	0	0
6 in ***1***	3.1	5.6	7.4
6 in ***5***	12.9	15.1	14.3

[a]single point calculations using the PBE-TS optimised structures, [b]fixed cell optimisation using the PBE-TS optimised structures. For details see section 4.9.

3. Conclusions

2-Mercaptoimidazolium salts remain a very interesting and challenging class of compounds, exhibiting intriguing physico-chemical properties. Even though the investigated molecules show conformational flexibility only two conformations were observed among the compounds, with the conformations being related to either the global minimum or a low energy local minimum.

Exchanging the counterion (Cl^- ↔ Br^-), as exemplarily investigated for the racemic imidazo-thiazinium salts, leads to isostructural packing arrangements, as seen for other compounds.[52-57] The substitution of Cl^- by Br^- hardly affects the

thermal behavior of the compounds, but increases the moisture dependent stability (deliquescence occurs at higher RH values) as well as the solubility in DMSO. Distinct packing arrangements were observed by replacing the imidazole moiety of the cation by a triazole or tetrazole moiety. Nevertheless, computational substitution calculations, *i.e.* replacing one cation by the other in the same structure, revealed that isostructural packing arrangements are thermodynamically feasible, albeit higher in lattice energy. Thus, templating experiments[58, 59] may be a successful route to polymorphs of the racemic triazolo- and tetrazolo-thiazinium bromides.

The experimental and computational investigations on the enantiopure and racemic compounds of the imidazo-thiazinium chloride confirmed the presence of a racemic crystal and revealed that there is a strong driving force for racemisation, making handling of the enantiopure crystals challenging at ambient conditions. The computational results are promising, as the computed energy differences agree reasonably well with the measured values (DSC), and the pairwise intermolecular interaction energy calculations (frameworks) provide an explanation, why the homochiral crystal packing arrangement is of lower stability than the racemic crystal.

To conclude, this study demonstrates the benefit of complementary experimental and computational approaches to improve the understanding of the relationships between structural features and thermodynamic properties of chiral compounds.

4. Materials and Methods

4.1. Materials

Starting materials, solvents, and reagents were purchased from Sigma-Aldrich, St. Louis, Mo., USA (European affiliate Steinheim, D) and were used without further purification. The D6-DMSO used for the NMR analyses was purchased from Eurisotop (Saint-Aubin, F). The solvent was shipped in 10 ml septum vials and had an isotopic purity of 99.8 % D and an initial water content of <0.02 %.

4.2. Synthetic procedures

(*RS*)-6-Hydroxy-1-methyl-1,5,6,7-tetrahydroimidazo[2,1-b][1,3]thiazinium bromide (*1*, *RS*-Br). To a solution of 2-mercapto-1-methylimidazole (2.0 g, 17.5 mmol) in dichloromethane (100 mL) (*rac*)-epibromohydrin (1.6 mL, 18.7 mmol) was added. The mixture was stirred for three days at room temperature (RT). The formed precipitate was filtered, washed twice with dichloromethane (2x 10 mL) and dried under reduced pressure, yielding 3.3 g (75 %) of (*RS*)-6-hydroxy-1-methyl-1,5,6,7-tetrahydroimidazo[2,1-b][1,3]thiazinium bromide (***1***) as a white powder. Single crystals were obtained by slowly cooling a solution of compound ***1*** (100 mg) in a minimal amount of hot methanol to RT. The solution was then stored at 5 °C. After a few days, single crystals were collected by decantation of the supernatant. – Bulk purity based on solvent-corrected NMR-integrals: >98 % – M.p. 173.5 °C – ***^{1}H-NMR*** (300 MHz, [D6]DMSO): δ = 3.41 (dd, *J* = 12.7, 5.1 Hz, 1H, S-CH_2), 3.56 (dd, *J* = 12.6, 2.0 Hz, 1H, S-CH_2), 3.66 (s, 3H, Me), 4.20 (d, *J* = 3.1 Hz, 2H, N-CH_2), 4.52 – 4.58 (m, 1H, CH), 5.89 (br s, 1H, OH), 7.72 (s, 2H, Im) ppm. – ***^{13}C-NMR*** (75 MHz, [D_6]DMSO): δ = 31.7 (Me), 34.0 (S-CH_2), 51.5 (N-CH_2), 58.0 (CH), 122.6 (Im), 123.2 (Im), 140.3 (Im) ppm. – ***FT-IR*** *(ATR): v* = 3273 (br m) (*v*OH), 3083 (m), 3064 (m), 2996 (w), 2970 (w) (*v*CH, *v*CH_2, *v*CH_3, *v*S-CH_2), 1661 (w), 1570 (m), 1516 (m) (*v*C=N, *v*C=C), 1478 (m), 1449 (m), 1412 (m), 1349 (m), 1311 (m) (δCH_2, δCH_3), 1275 (s), 1219 (s) (δ_iOH), 1187 (m), 1151 (m), 1098 (m) (*v*CC, $\delta_i CH_{ar}$), 1078 (s) (*v*CO), 807 (m), 784 (s), 660 (s), 627 (s), 604 (s) (*v*CC, $\delta_o CH_{ar}$), 475 (s) cm^{-1}.

(*RS*)-6-Hydroxy-1-methyl-1,5,6,7-tetrahydroimidazo[2,1-b][1,3]thiazinium chloride (2, *RS*-**Cl).** To a solution of 2-mercapto-1-methylimidazole (2.0 g, 17.5 mmol) in acetonitrile (20 mL) (*rac*)-epichlorohydrin (1.5 mL, 19.1 mmol) was added. The mixture was stirred for three days under reflux conditions. The formed precipitate was filtered, washed twice with acetonitrile (2x 10 mL) and dried under reduced pressure, yielding 2.7 g (75 %) of (*RS*)-6-hydroxy-1-methyl-1,5,6,7-tetrahydroimidazo[2,1-b][1,3]thiazinium chloride (***2***) as a white powder. Single crystals of ***2*** were obtained as described for ***1***. – Bulk purity based on solvent-corrected NMR-integrals: >98 % – M.p. 178.9 °C – ***^{1}H-NMR*** (300 MHz, [D_6]DMSO): δ = 3.43 (dd, *J* = 12.8, 5.1 Hz, 1H, S-CH_2), 3.55 (dd, *J* = 12.6, 2.0 Hz, 1H, S-CH_2), 3.66 (s, 3H, Me), 4.20 (d, *J* = 2.6 Hz, 2H, N-CH_2), 4.50 – 4.58 (m, 1H, CH), 6.21 (br s, 1H, OH), 7.73 (s, 2H, Im) ppm. – ***^{13}C-NMR*** (75 MHz, [D_6]DMSO): δ = 31.7 (Me), 33.9 (S-CH_2), 51.5 (N-CH_2), 58.0 (CH), 122.6 (Im), 123.2 (Im), 140.3 (Im) ppm. – ***FT-IR*** *(ATR): v* = 3204 (br m) (*v*OH), 3084 (m), 3065 (m), 3000 (w), 2971 (w) (*v*CH, *v*CH_2, *v*CH_3, *v*S-CH_2), 1677 (w), 1569 (m), 1519 (m) (*v*C=N, *v*C=C), 1480 (m), 1453 (m), 1413 (m), 1350 (m), 1311 (m) (δCH_2, δCH_3), 1278 (s), 1222 (m) (δ_iOH), 1189 (m), 1153 (m), 1099 (m) (*v*CC, $\delta_i CH_{ar}$), 1082 (s) (*v*CO), 808 (m), 795 (s), 686 (s), 659 (s), 600 (m) (*v*CC, $\delta_o CH_{ar}$), 477 (s) cm^{-1}.

This compound has been reported by Press *et al.*[27], however, it was synthesised *via* an alternative approach resulting in low yields (10 %) and/or in a mixture with NaCl. The reported analytical data agree with the values reported in this study.

(*R*)-6-Hydroxy-1-methyl-1,5,6,7-tetrahydroimidazo[2,1-b][1,3]thiazinium chloride (3, *R*-**Cl).** To a solution of 2-mercapto-1-methylimidazole (2.5 g, 21.9 mmol) in anhydrous acetonitrile (30 mL) (*S*)-(+)-epichlorohydrin (1.7 mL, 21.7 mmol) was added. The mixture was stirred under argon for three days under reflux conditions. Cooling to RT without stirring led to the separation of the product as an amorphous oily phase which crystallised upon prolonged standing. The upper layer was decanted, the solid was washed with ether (10mL), filtered under inert gas, dried *in vacuo* and stored under argon, yielding 3.1 g (69 %) of (*R*)-6-hydroxy-1-methyl-1,5,6,7-tetrahydroimidazo [2,1-b][1,3]thiazinium chloride (**3**) as an off-white solid. Single crystals were obtained by storing the decanted supernatant at –24 °C for three days. – Bulk purity based on solvent-corrected NMR-integrals: >96 % – M.p. 126.2 °C – ***^{1}H-NMR*** (300 MHz, [D_6]DMSO): δ = 3.44 (dd, *J* = 12.7, 4.9 Hz, 1H, S-CH_2), 3.56 (dd, *J* = 12.6, 2.1 Hz, 1H, S-CH_2), 3.66 (s, 3H, Me), 4.19 – 4.24 (m, 2H, N-CH_2), 4.48 – 4.59 (m, 1H, CH), 6.26 (br s, 1H, OH), 7.75 (s, 2H, Im) ppm.

– ***^{13}C-NMR*** (75 MHz, [D_6]DMSO): δ = 31.7 (Me), 33.9 (S-CH_2), 51.5 (N-CH_2), 58.0 (CH), 122.6 (Im), 123.2 (Im), 140.3 (Im) ppm. – ***FT-IR*** *(ATR):* ν = 3189, 3148 (br m) (νOH), 3101 (m), 2989 (w), (νCH, νCH_2, νCH_3, νS-CH_2), 1630 (w), 1569 (m), 1515 (m) (νC=N, νC=C), 1480 (m), 1447 (m), 1424 (m), 1343 (m), 1325 (m) (δCH_2, δCH_3), 1290 (m), 1268 (m), 1210 (s) (δ_iOH), 1180 (m), 1149 (w) (νCC, $\delta_i CH_{ar}$), 1086 (s) (νCO), 808 (m), 764 (s), 655 (s), 602 (s) (νCC, $\delta_o CH_{ar}$), 469 (m) cm^{-1}.

(*S*)-6-Hydroxy-1-methyl-1,5,6,7-tetrahydroimidazo[2,1-b][1,3]thiazinium chloride (*4*, *S*-Cl). To a solution of 2-mercapto-1-methylimidazole (2.5 g, 21.9 mmol) in anhydrous acetonitrile (30 mL) (*R*)-(+)-epichlorohydrin (1.7 mL, 21.7 mmol) was added. The mixture was stirred under argon for three days under reflux conditions. Upon cooling to RT and continued stirring (in contrast to ***3***), an off-white precipitate was formed, which was Schlenk-filtered, dried under reduced pressure and stored under argon, yielding 3.0 g (67 %) of (*S*)-6-hydroxy-1-methyl-1,5,6,7-tetrahydroimidazo[2,1-b][1,3]thiazinium chloride (***4***). – Bulk purity based on solvent-corrected NMR-integrals: >94 % – M.p. 126.1 °C – ***^{1}H-NMR*** (300 MHz, [D_6]DMSO): δ = 3.43 (dd, *J* = 12.7, 4.8 Hz, 1H, S-CH_2), 3.55 (dd, *J* = 12.6, 1.9 Hz, 1H, S-CH_2), 3.66 (s, 3H, Me), 4.20 (d, *J* = 2.2 Hz, 2H, N-CH_2), 4.49 – 4.57 (m, 1H, CH), 6.20 (br s, 1H, OH), 7.73 (s, 2H, Im) ppm. – ***^{13}C-NMR*** (75 MHz, [D_6]DMSO): δ = 31.7 (Me), 33.9 (S-CH_2), 51.5 (N-CH_2), 58.0 (CH), 122.6 (Im), 123.2 (Im), 140.3 (Im) ppm. – ***FT-IR*** *(ATR):* ν = 3149 (br m) (νOH), 3068 (m), 3000 (w), 2971 (w) (νCH, νCH_2, νCH_3, νS-CH_2), 1641 (m), 1569 (m), 1520 (m) (νC=N, νC=C), 1481 (m), 1456 (m), 1419 (m), 1347 (m), 1315 (m) (δCH_2, δCH_3), 1248 (s), 1222 (m) (δ_iOH), 1190 (m), 1154 (m) (νCC, $\delta_i CH_{ar}$), 1088 (s) (νCO), 810 (m), 773 (s), 659 (s), 602 (m) (νCC, $\delta_o CH_{ar}$), 475 (m) cm^{-1}.

(*RS*)-6-Hydroxy-3-methyl-3,5,6,7-tetrahydro[1,2,4]triazolo[5,1-b][1,3]thiazinium bromide (*5*). (*rac*)-Epibromohydrin (2.5 mL, 29.2 mmol) was added to a solution of 3-mercapto-4-methyl-4*H*-1,2,4-triazole (3.0 g, 26.1 mmol) in acetonitrile (40 mL). The mixture was stirred under argon for 18 h, forming a white precipitate. The formed precipitate was filtered, the solid was washed twice with acetonitrile (2x 10 mL) and dried under reduced pressure. Yield: 4.7 g (72 %) of (*RS*)-6-hydroxy-3-methyl-3,5,6,7-tetrahydro[1,2,4]triazoleo[5,1-b][1,3]thiazinium bromide (***5***) as a white crystalline solid. Single crystals of ***5*** were obtained as described for ***1*** – Bulk purity based on solvent-corrected NMR-integrals: >97 % – ***^{1}H-NMR*** (300 MHz, [D_6]DMSO): δ = 3.49 – 3.65 (m, 2H, S-CH_2), 3.72 (s, 3H, Me), 4.24 – 4.43 (m, 2H, N-CH_2), 4.64 – 4.72 (m, 1H, CH), 6.04 (d, *J* = 3.9 Hz, 1H, OH), 9.13 (s, 1H, CH_{ar}) ppm. – ***^{13}C-NMR*** (75 MHz, [D6]DMSO): δ = 32.5 (Me), 32.6 (S-CH2), 54.1 (N-CH2), 58.5 (CH), 144.3 (CH_{ar}), 149.2 (C_{ar}) ppm. – ***FT-IR*** *(ATR):* ν = 3272 (br m) (νOH), 3111 (m), 3060 (m), 2971 (m), 2880 (w) (νCH, νCH_2, νCH_3, νS-CH_2), 1550 (m), 1525 (s) (νC=N, νC=C), 1460 (m), 1442 (m), 1400 (m), 1361 (m), 1332 (m) (δCH_2, δCH_3), 1286 (m), 1222 (s) (δ_iOH), 1173 (m) (νCC), 1090 (s) (νCO), 1039 (s), 943 (m), 889 (m), 867 (s), 805 (s), 722 (m), 661 (m), 633 (s), 611 (s) (νCC) cm^{-1}.

(*RS*)-6-Hydroxy-3-methyl-3,5,6,7-tetrahydrotetrazolo[5,1-b][1,3]thiazinium bromide (*6*). (*rac*)-Epibromohydrin (2 mL, 23.4 mmol) was added to a solution of 5-mercapto-1-methyltetrazole (2.5 g, 21.5 mmol) in acetonitrile (20 mL). The mixture was stirred for 24 h under inert gas. Diethyl ether (20 mL) was added after cooling to RT, forming a white precipitate. It was filtered, washed twice with diethyl ether (2x 10 mL) and dried under reduced pressure, yielding 2.2 g (58 %) of (*RS*)-6-hydroxy-3-methyl-3,5,6,7-tetrahydrotetrazoleo[5,1-b][1,3]thiazinium bromide (***6***) as a white crystalline solid. Single crystals of ***6*** were obtained as described for ***1***. – Bulk purity based on solvent-corrected NMR-integrals: >94 % – ***^{1}H-NMR*** (300 MHz, [D_6]DMSO): δ = 3.61 – 3.67 (m, 2H, S-CH_2), 4.15 (s, 3H, Me), 4.55 – 4.63 (m, 1H, CH), 4.70 – 4.84 (m, 2H, N-CH_2), 6.18 (d, *J* = 3.7 Hz, 1H, OH) ppm. – ***^{13}C-NMR*** (75 MHz, [D_6]DMSO): δ = 33.8 (Me), 35.8 (S-CH_2), 53.4 (N-CH_2), 57.9 (CH), 151.7 (C_{ar}) ppm. – ***FT-IR*** *(ATR):* ν = 3216 (br s) (νOH), 3016 (w), 2981 (w), 2949 (w), 2906 (w) (νCH_2, νCH_3, νS-CH_2), 1516 (s), 1489 (m) (νC=N, νC=C), 1420 (m), 1412 (m), 1370 (m), 1336 (m), 1323 (m) (δCH_2, δCH_3), 1299 (m), 1280 (s) (δ_iOH), 1201 (m), 1171 (m), 1099 (m) (νCC), 1077 (s) (νCO), 1036 (m), 1015 (m), 893 (m), 818 (m), 728 (m), 650 (s), 636 (s) (νCC) cm^{-1}.

^{1}H-NMR, ^{13}C-NMR and IR spectra of ***1*** – ***6*** can be found in section 1 of the ESI.

4.3. Thermal analysis

For *hot-stage microscopic* (HSM) investigations a Reichert Thermovar polarisation microscope, equipped with a Kofler hot-stage (Reichert, A), was used.

Differential Scanning Calorimetry (DSC) thermograms were recorded on a DSC 7 (Perkin-Elmer Norwalk, Ct., USA) controlled by the Pyris 2.0 software. Using a UM3 ultramicrobalance (Mettler, Greifensee, CH), samples of approximately 3 - 5 mg were weighed into perforated aluminium pans or high-pressure capsules. The samples were heated in closed crucibles using rates of 10 °C min^{-1} with dry nitrogen as the purge gas (purge: 20 mL min^{-1}). The instrument was calibrated for temperature with pure benzophenone (mp 48.0 °C) and caffeine (236.2 °C), and the energy calibration was performed with indium (mp 156.6 °C, heat of fusion 28.45 J g^{-1}). The errors on the stated temperatures and enthalpy values were calculated at the 95% confidence interval levels and are based on three measurements.

4.4. X-ray diffraction

Powder X-ray diffraction patterns were obtained using a X'Pert PRO diffractometer (PANalytical, Almelo, Netherlands) equipped with a θ/θ coupled goniometer in transmission geometry and a programmable XYZ stage with well plate holder. A Cu$K\alpha_{1,2}$ radiation source with a focussing mirror, a 0.5° divergence slit and a 0.02° Soller slit collimator on the incident beam side, a 2 mm anti-scattering slit and a 0.02° Soller slit collimator on the diffracted beam side and a solid state PIXcel detector were used. The patterns were recorded at a tube voltage of 40 kV, tube current of 40 mA, applying a step size of 2θ = 0.013° with 40 s per step in the 2θ range between 2° and 40°.

Single-crystal X-ray diffraction. Data collection for ***1*** and ***2*** was carried out on a Nonius Kappa CCD diffractometer (Bruker,

Billerica, Ma., USA) using graphite-monochromated Mo-K_α radiation (λ = 0.71073 Å). The ***3***, ***5*** and ***6*** data set (MoK_α radiation) were collected on an Oxford Diffraction Gemini-R Ultra diffractometer operated by the CrysAlis software.[60] The structures were solved by direct methods (SIR2011)[61] and refined by full-matrix least squares on F^2 using SHELXL2013[62] and the program package WinGX[63]. All non-hydrogen atoms were refined anisotropically. The hydroxyl hydrogen atoms, located in difference maps, were refined with distance restraints. All hydrogen atoms bound to carbon atoms were generated by a riding model in idealised geometries and their positions refined with U_{iso}(H) = 1.5 U_{eq}(C) for –CH_3 groups and U_{iso}(H) = 1.2 U_{eq}(C) for other H atoms. Precession-type reconstructions of reciprocal space revealed the presence of non-merohedral twinning for crystals of ***3***. Indeed, the reciprocal lattices of the two twin domains were related by a rotation of 180° about the crystallographic c-axis. The diffraction spots belonging to both domains were indexed in CrysAlisPro and raw data were processed to give an hklf 5 formatted file.

4.5. Gravimetric moisture sorption/desorption analysis

Automated moisture sorption and desorption studies were performed with the automatic multisample gravimetric moisture sorption analyser SPS23-10µ (ProUmid, Ulm, D). The moisture sorption analyser was calibrated with saturated salt solutions according to the suppliers' recommendations. Approximately 100–150 mg of sample was used for each analysis. The measurement cycles were started at 0%, followed by a sorption cycle (increasing humidity) up to 90% and a desorption cycle (decreasing humidity) to 0%. The RH changes were set to 10%. The equilibrium condition for each step was set to a mass constancy of ±0.003% over 60 minutes and a maximum time limit of 48 hours per step.

4.6. Solubility measurements

The Crystal16 crystallisation system (Technobis, NL) was used to determine the solubility in DMSO. The temperature at the point the suspension becomes a clear solution upon heating or the "clear point" (at 0.1 °C per minute) was taken as the saturation temperature of the measured sample with known concentration.

4.7. Potential energy surface (PES) scans

PES scans were performed at the B3LYP/6-31G(d,p), PBE0/6-31G(d,p) and MP2/6-31G(d,p) levels using GAUSSIAN09.[64] The dihedral angle H–O–C3–C4 (Fig. 1) for each of the three cations and each two low energy ring conformations, was scanned in 20° steps.

4.8. Intermolecular energy calculations

Pairwise energy contributions were calculated using CrystalExplorer V17.[43, 65, 66] The optimised atomic positions (PBE-TS, see next section) were used for the calculations (radius 5 Å). The model energies have been calculated between all unique nearest neighbour ion pairs. The used model (CE-B3LYP) uses B3LYP/6-31G(d,p) molecular wave functions calculated by applying the molecular geometries extracted from the crystal structures. This approach uses electron densities of unperturbed monomers to obtain four separate energy components: electrostatic (E_E), polarisation (E_P), dispersion (E_D), and exchange-repulsion (E_R). Each energy term was scaled independently to fit a large training set of B3LYP-D2/6-31G(d,p) counterpoise-corrected energies from both organic and inorganic crystals.[43]

4.9. Periodic DFT-d calculations

Initial DFT-d calculations were carried out with the CASTEP plane wave code V6.1[67] using the Perdew-Burke-Ernzerhof (PBE) generalised gradient approximation (GGA) exchange-correlation density functional[68] and ultrasoft pseudopotentials,[69] with the addition of the Tkatchenko and Scheffler (TS)[70] semi-empirical dispersion correction. Brillouin zone integrations were performed on a symmetrised Monkhorst–Pack grid with the number of *k*-points chosen to provide a maximum spacing of $2\pi \cdot 0.07$ Å^{-1} and a basis set cut-off of 560 eV. The self-consistent field convergence on total energy was set to $1 \cdot 10^{-5}$ eV. Energy minimisations were performed using the Broyden–Fletcher–Goldfarb–Shanno optimisation scheme within the space group constraints. The optimisations were considered complete when energies were converged to better than $2 \cdot 10^{-5}$ eV per atom, atomic displacements converged to $1 \cdot 10^{-3}$ Å, maximum forces converged to $5 \cdot 10^{-2}$ eV Å^{-1}, and maximum stresses were converged to 0.1 GPa. Starting from the PBE-TS optimised structures single point calculations were performed using the Tkatchenko and Scheffler (TS)[70] or Grimme D2[71] semi-empirical dispersion correction, *k*-point settings to provide a maximum spacing of $2\pi \cdot 0.04$ Å^{-1} and a basis set cut-off of 780 eV. Finally, fixed unit cell lattice energies optimisations (starting from PBE-TS) were undertaken, using Tkatchenko-Scheffler's Many-Body Dispersion scheme (MBD*),[72] as implemented in CASTEP V19.11, with on-the-fly ultrasoft pseudopotentials, a plane wave cut-off energy of 1100 eV, *k*-point grid spacing of $2\pi \cdot 0.07$ Å^{-1}, an SCF electronic energy tolerance of 10^{-8} eV and force convergence tolerance criteria of 0.005 eV Å^{-1}.

Conflicts of interest

There are no conflicts to declare.

Acknowledgements

DEB would like to thank Sandoz GmbH, Kundl for financial support. The calculations have been performed using the HPC infrastructure LEO of the University of Innsbruck.

Notes and references

1. J. Jacques, A. Collet and S. H. Wilen, *Enantiomers, Racemates and Resolutions*, Krieger Publishing Company, Malabar, Florida, 1994.
2. J. M. Rollinger and A. Burger, *J. Pharm. Sci.*, 2001, **90**, 949-959.
3. T. Rekis, A. Berzins, D. Dzabijeva, I. Nakurte, L. Orola and A. Actins, *Cryst. Growth Des.*, 2017, **17**, 1814-1823.
4. J. D. Dunitz, *Acta Crystallographica Section B - Structural Science*, 1995, **51**, 619-631.

5. J. Bernstein, *Polymorphism in Molecular Crystals*, Clarendon Press, Oxford, 2002.
6. J. E. Rekoske, *AIChE Journal*, 2001, **47**, 2-5.
7. H. Lorenz, A. Perlberg, D. Sapoundjiev, M. P. Elsner and A. Seidel-Morgenstern, *Chem. Eng. Processing*, 2006, **45**, 863-873.
8. G. Coquerel, in *Novel Optical Resolution Technologies*, eds. K. Sakai, N. Hirayama and R. Tamura, Springer-Verlag, Berlin, 2007, ch. 1, pp. 1-51.
9. G. Coquerel and D. B. Amabilino, in *Chirality at the Nanoscale*, ed. D. B. Amabilino, Wiley-VCH, Weinheim, 2009, ch. 10, pp. 305-348.
10. A. Collet, L. Ziminski, C. Garcia and F. Vigné-Maeder, in *Supramolecular Stereochemistry*, ed. J. S. Siegel, Kluwer Academic Publishers, Netherlands, 1995, pp. 91-110.
11. A. Collet, *Enantiomer*, 1999, **4**, 157-172.
12. F. J. J. Leusen, J. H. Noordik and H. R. Karfunkel, *Tetrahedron*, 1993, **49**, 5377-5396.
13. Z. J. Li, M. T. Zell, E. J. Munson and D. J. W. Grant, *J. Pharm. Sci.*, 1999, **88**, 337-346.
14. U. S. Food and Drug Administration, *Development of New Stereoisomeric Drugs*, 1992.
15. A. Hantzsch and J. H. Weher, *Chem. Zentralbl.*, 1888, **59**, 94-96.
16. M. Hummel, M. Markiewicz, S. Stolte, M. Noisternig, D. E. Braun, T. Gelbrich, U. J. Griesser, G. Partl, B. Naier, K. Wurst, B. Kruger, H. Kopacka, G. Laus, H. Huppertz and H. Schottenberger, *Green Chem.*, 2017, **19**, 3225-3237.
17. L. Andreani and J. D. Rocha, *Braz. J. Chem. Eng.*, 2012, **29**, 1-13.
18. K. Seib and F. G. M. Vogel, *Soap, Cosmet., Chem. Spec.*, 1985, **61**, 34, 36-37, 54.
19. A. I. Siriwardana, I. R. Crossley, A. A. J. Torriero, I. M. Burgar, N. F. Dunlop, A. M. Bond, G. B. Deacon and D. R. MacFarlane, *J. Org. Chem.*, 2008, **73**, 4676-4679.
20. G. Laus, A. Schwaerzler, P. Schuster, G. Bentivoglio, M. Hummel, K. Wurst, V. Kahlenberg, T. Loerting, J. Schuetz, P. Peringer, G. Bonn, G. Nauer and H. Schottenberger, *Z. Naturforsch., B Chem. Sci.*, 2007, **62**, 295-308.
21. S. C. Shilcrat, M. K. Mokhallalati, J. M. D. Fortunak and L. N. Pridgen, *J. Org. Chem.*, 1997, **62**, 8449-8454.
22. T.-T. Tung, T. T. Dao, M. G. Junyent, M. Palmgren, T. Guenther-Pomorski, A. T. Fuglsang, S. B. Christensen and J. Nielsen, *ChemMedChem*, 2018, **13**, 37-47.
23. M. C. Aragoni, M. Arca, F. Demartin, A. Devillanova Francesco, A. Garau, F. Isaia, V. Lippolis and G. Verani, *J. Am. Chem. Soc.*, 2002, **124**, 4538-4539.
24. W.-W. du Mont, G. Mugesh, C. Wismach and P. G. Jones, *Angew. Chem., Int. Ed.*, 2001, **40**, 2486-2489.
25. A. Taurog, *Endocrinology*, 1976, **98**, 1031-1046.
26. J.-X. Gong, Y. He, Z.-L. Cui and Y.-W. Guo, *Phosphorus, Sulfur Silicon Relat. Elem.*, 2016, **191**, 1036-1041.
27. J. B. Press, J. J. McNally, Z. G. Hajos and R. A. Sawyers, *J. Org. Chem.*, 1992, **57**, 6335-6339.
28. H. Alper and E. C. H. Keung, *J. Org. Chem.*, 1972, **37**, 1464-1466.
29. H. Alper and R. W. Stout, *J. Heterocycl. Chem.*, 1973, **10**, 569-574.
30. M. R. Aouad, N. Rezki and E. S. H. El Ahsry, *J. Heterocycl. Chem.*, 2008, **45**, 1321-1327.
31. M. L. Glowka, *J. Chem. Crystallogr.*, 1994, **24**, 273-276.
32. M. L. Glowka, H. Foks and W. Rudnicka, *J. Chem. Crystallogr.*, 1994, **24**, 527-530.
33. L. El Ouasif, M. El Ghoul, R. Achour, M. Saadi and L. El Ammari, *IUCrData*, 2017, **2**, x170429.
34. E. S. Il'inykh, D. G. Kim, M. I. Kodess, E. G. Matochkina and P. A. Slepukhin, *J. Fluorine Chem.*, 2013, **149**, 24-29.
35. M. Yoneda, K. Tanaka, T. Fujiwara and K. Tomita, *Acta Crystallogr., Sect. B*, 1979, **B35**, 2355-2358.
36. M. A. Orlov, I. V. Kapitanov, N. I. Korotkikh and O. P. Shvaika, *Chem. Heterocycl. Compd.* , 2014, **50**, 111-116.
37. M. A. Orlov, A. F. Aslanov and N. I. Korotkikh, *Chem. Heterocycl. Compd.*, 2010, **46**, 347-350.
38. H. G. Brittain, S. J. Bogdanowich, D. E. Bugay, J. Devincentis, G. Lewen and A. W. Newman, *Pharm. Res*, 1991, **8**, 963-973.
39. R. Hilfiker, *Polymorphism in the Pharmaceutical Industry*, Wiley-VCH, Weinheim, 2006.
40. N. Chieng, T. Rades and J. Aaltonen, *J. Pharm. Biomed. Anal.*, 2011, **55**, 618-644.
41. A. Authier, *International Tables for Crystallography: Volume D*, John Wiley & Sons, 2014.
42. J. A. Chisholm and S. Motherwell, *J. Appl. Crystallogr.*, 2005, **38**, 228-231.
43. C. F. Mackenzie, P. R. Spackman, D. Jayatilaka and M. A. Spackman, *IUCrJ*, 2017, **4**.
44. C. P. Brock, W. B. Schweizer and J. D. Dunitz, *JACS*, 1991, **113**, 9811-9820.
45. D. E. Braun, M. Ardid-Candel, E. D'Oria, P. G. Karamertzanis, J. B. Arlin, A. J. Florence, A. G. Jones and S. L. Price, *Cryst. Growth Des.*, 2011, **11**, 5659-5669.
46. E. D'Oria, P. G. Karamertzanis and S. L. Price, *Cryst. Growth Des.*, 2010, **10**, 1749-1756.
47. H. K. Buchholz, R. K. Hylton, J. G. Brandenburg, A. Seidel-Morgenstern, H. Lorenz, M. Stein and S. L. Price, *Cryst. Growth Des.*, 2017, **17**, 4676-4686.
48. Y. Cao, Y. Chen, X. Sun, Z. Zhang and T. Mu, *PCCP*, 2012, **14**, 12252-12262.
49. Z. Ba, G. Huang, D. Qiao and D. Feng, *Appl. Surf. Sci.*, 2020, **529**, 147031.
50. J. B. Arlin, L. S. Price, S. L. Price and A. J. Florence, *Chem. Commun.*, 2011, **47**, 7074-7076.
51. D. H. Case, V. K. Srirambhatla, R. Guo, R. E. Watson, L. S. Price, H. Polyzois, J. K. Cockcroft, A. J. Florence, D. A. Tocher and S. L. Price, *Cryst. Growth Des.*, 2018, **18**, 5322-5331.
52. W. Prukala, D. Prukala and M. Kubicki, *Acta Crystallogr., Sect. C Cryst. Struct. Commun.*, 2008, **64**, o269-o271.
53. C. Tamuly, R. S. Sarma, A. S. Batsanov, A. E. Goeta and J. B. Baruah, *Acta Crystallogr., Sect. C Cryst. Struct. Commun.*, 2005, **C61**, o324-o327.
54. C. Borel and A. D. Bond, *Acta Crystallogr., Sect. E Struct. Rep. Online*, 2008, **64**, o34, o34/31-o34/36.
55. K. Sankovic, B. Prugovecki and D. Matkovic-Calogovic, *Acta Crystallogr., Sect. E Struct. Rep. Online*, 2005, **61**, o3846-o3848.
56. A. M. Owczarzak, N. Kourkoumelis, S. K. Hadjikakou and M. Kubicki, *CrystEngComm*, 2013, **15**, 3607-3614.
57. S. Faeth, M. Vilsmeier and A. Pfitzner, *Z. Naturforsch., B J. Chem. Sci.*, 2019, **74**, 119-124.
58. N. Zencirci, T. Gelbrich, V. Kahlenberg and U. J. Griesser, *Cryst. Growth Des.*, 2009, **9**, 3444-3456.
59. V. K. Srirambhatla, A. J. Florence, R. Guo and S. L. Price, *Chem. Commun.*, 2016, **52**, 7384-7386.
60. *Journal*, 2006.
61. M. C. Burla, R. Caliandro, M. Camalli, B. Carrozzini, G. L. Cascarano, C. Giacovazzo, M. Mallamo, A. Mazzone, G. Polidori and R. Spagna, *J. Appl. Crystallogr*, 2012, **45**, 357-361.
62. G. M. Sheldrick, *Acta Crystallogr. , Sect. C: Struct. Chem*, 2015, **71**, 3-8.

63. L. J. Farrugia, *J. Appl. Crystallogr*, 2012, **45**, 849-854.
64. M. J. Frisch, G. W. Trucks, H. B. Schlegel, G. E. Scuseria, J. M. A. Robb, R. Cheeseman, G. Scalmani, V. Barone, B. Mennucci, G. A. Petersson, H. Nakatsuji, M. Caricato, X. Li, H. P. Hratchian, A. F. Izmaylov, J. Bloino, G. Zheng, J. L. Sonnenberg, M. Hada, M. Ehara, K. Toyota, R. Fukuda, J. Hasegawa, M. Ishida, T. Nakajima, Y. Honda, O. Kitao, H. Nakai, T. Vreven, J. A. Montgomery, J. E. Peralta, F. Ogliaro, M. Bearpark, J. J. Heyd, E. Brothers, K. N. Kudin, V. N. Staroverov, R. Kobayashi, J. Normand, K. Raghavachari, A. Rendell, J. C. Burant, S. S. Iyengar, J. Tomasi, M. Cossi, N. Rega, J. M. Millam, M. Klene, J. E. Knox, J. B. Cross, V. Bakken, C. Adamo, J. Jaramillo, R. Gomperts, R. E. Stratmann, O. Yazyev, A. J. Austin, R. Cammi, C. Pomelli, J. W. Ochterski, R. L. Martin, K. Morokuma, V. G. Zakrzewski, G. A. Voth, P. Salvador, J. J. Dannenberg, S. Dapprich, A. D. Daniels, O. Farkas, J. B. Foresman, J. V. Ortiz, J. Cioslowski and D. J. Fox, *Gaussian 09, Gaussian Inc.. Wallingford CT*, 2009.
65. M. J. Turner, S. Grabowsky, D. Jayatilaka and M. A. Spackman, *J. Phys. Chem. Lett.*, 2014, **5**, 4249-4255.
66. M. J. Turner, S. P. Thomas, M. W. Shi, D. Jayatilaka and M. A. Spackman, *Chem. Commun.* , 2015, **51**, 3735-3738.
67. S. J. Clark, M. D. Segall, C. J. Pickard, P. J. Hasnip, M. J. Probert, K. Refson and M. C. Payne, *Z. Kristallogr.*, 2005, **220**, 567-570.
68. J. P. Perdew, K. Burke and M. Ernzerhof, *Phys. Rev. Lett.*, 1996, **77**, 3865-3868.
69. D. Vanderbilt, *Physical Review B*, 1990, **41**, 7892-7895.
70. A. Tkatchenko and M. Scheffler, *Phys. Rev. Lett.*, 2009, **102**, 073005/073001-073005/073004.
71. S. Grimme, *J. Comput. Chem*, 2006, **27**, 1787-1799.
72. A. Ambrosetti, A. M. Reilly, R. A. Di Stasio and A. Tkatchenko, *J. Chem. Phys.*, 2014, **140**, 18A508/501-518A508/514.